Phase State Effect on Adhesion Behavior of Self-Assembled Monolayers

Dae Ho Lee, Dohwan Kim, Taebyoung Oh, and Kilwon Cho*

Department of Chemical Engineering, School of Environmental Science and Engineering, Polymer Research Institute, Pohang University of Science and Technology, Pohang 790-784, South Korea

Received March 3, 2004

The effect of phase state of self-assembled monolayers (SAMs) on adhesion behavior was studied using a combination of atomic force microscopy (AFM) and Johnson−Kendall−Roberts (JKR) methods. The phase state of SAMs was controlled by adjusting the reaction temperature. Order-to-disorder structural transitions in monolayers of *n*-alkyltrichlorosilanes resulted in dramatic increases in adhesion force and adhesion hysteresis, which represents the first report of alterations in adhesion properties due to phase changes of monolayers without any effect of chain length and surface heterogeneity. This increase in mechanical deformation of the disordered monolayer is understood to be caused by increases in (1) molecular contact between the AFM tip and a disordered monolayer due to the more deformable state of the latter and (2) monolayer deformation during unloading by the JKR probe lens. Adhesion hysteresis was found to have greater sensitivity toward the unloading rate for disordered monolayers. The occurrence of maximum hysteresis at faster rates proves that monolayer chain mobility increases with structural disorder, resulting in increased mechanical deformation.

Introduction

Nano-adhesion has become an important issue with respect to the increasing need for miniaturized devices such as thin-film transistors, MEMS devices, and bio-interfaces.[1−5] Adhesion is associated with the intermolecular forces (physical/chemical) that occur between the interfacial atoms or molecules of the two materials at the mutual point of contact. Such intermolecular forces are the origin of surface energy or interfacial energy of materials. The strength of adhesion is intrinsically governed by the thermodynamic or intrinsic work of adhesion (W), which is defined in terms of both surface energy (γ_1, γ_2) and interfacial energy (γ_{12}), as $W = \gamma_1 + \gamma_2 - \gamma_{12}$ (Dupré equation).[6] However, in most situations, the intrinsic work of adhesion is essentially masked by the energy consumed by the mechanical deformation (viscoelastic or plastic deformation) of the adhesive or adherend itself. Generally, the dissipated energy (Φ) released from the mechanical deformation involved in the practical adhesion strength (G) is represented by $G = W(1+\Phi(v, T))$, where Φ is dimensionless quantity which is a function of v (rate) and T (temperature).[7,9,15,33,34] Due to the unstable (nonequilibrium) nature of the disordered monolayer during mechanical deformation, the dissipated energy is essentially time and temperature dependent and often much larger than the intrinsic work of adhesion. The Φ contribution at the nanoscale is important for the investigation of nanoadhesion.

Extensive work has been performed on the nanoadhesion or nanofriction behavior of the well-defined self-assembled monolayer (SAM) structure using atomic force microscopy (AFM), and Johnson-Kendall-Roberts (JKR), and surface force (SFA) methods. It has been revealed that structural changes in SAMs (e.g., chain length, packing density, and phase states (ordered/disordered)) have a significant effect on the adhesion or friction properties.[8−17]

A systematic study of the effect of phase state on the adhesion behavior in both ordered (crystalline) and disordered (amorphous/liquidlike) SAMs was previously reported by Israelachvili et al.[8] They described increases in adhesion hysteresis (i.e., $G - W$) in terms of the ability of the monolayer chains to rearrange and to enhance the molecular contact across the interphase (e.g., interdigitation). The authors reported large and small adhesion hystereses for amorphous monolayers, and for crystalline and liquidlike monolayers, respectively. However, in their

* To whom all correspondence should be addressed. E-mail: kwcho@postech.ac.kr.

(1) Stutzmann, N.; Friend, R. H.; Sirringhaus, H. *Science* **2003**, *299*, 1881.
(2) Kagan, C. R.; Mitzi, D. B.; Dimitrakopoulos, C. D. *Science* **2000**, *286*, 945.
(3) Srinivasan, U.; Houston, M. R.; Howe, R. T.; Maboudian, R. *J. Microelectromech. Syst.* **1998**, *7*, 252.
(4) López, G. P.; Albers, M. W.; Schreiber, S. L.; Carroll, R.; Peratta, E.; Whitesides, G. M. *J. Am. Chem. Soc.* **1993**, *115*, 5877.
(5) Willner, I.; Schlittner, A.; Doron, A.; Joselevich, E. *Langmuir* **1999**, *15*, 2766.
(6) Dupré, A. *Théorie Méchanique de la Chaleur*; Gauthier-Villars: Paris, 1869; p 369.
(7) (a) Kinloch, A. J. *Adhesion and adhesives*; Chapman and Hall: New York, 1987; p 270. (b) Ghatak, A.; Vorvolakos, K.; She, H.; Malotky, D. L.; Chaudhury, M. K. *J. Phys. Chem. B.* **2000**, *104*, 4018. (c) Ruths, M.; Granick, S. *Langmuir* **1998**, *14*, 1804. (d) Ruths, M.; Granick, S. *J. Phys. Chem. B.* **1998**, *102*, 6056. (e) Barthel, E.; Roux, S. *Langmuir* **2000**, *16*, 8134. (f) Bistac, S. *J. Colloid Interface Sci.* **1999**, *219*, 210.
(8) Chen, Y. L.; Helm, C. A.; Israelachvili, J. N. *J. Phys. Chem.* **1991**, *95*, 10736.
(9) van der Vegte, E. W.; Subbotin, A.; Hadziioannou, G. *Langmuir* **2000**, *16*, 3249.
(10) Nakagawa, T.; Ogawa, K.; Kurumizawa, T. *J. Vac. Sci. Technol. B* **1994**, *12*, 2215.
(11) (a) Xiao, X.; Hu, J.; Charych, D. H.; Salmeron, M. *Langmuir* **1996**, *12*, 235. (b) Leggett, G. J. *Anal. Chim. Acta* **2003**, *479*, 17.
(12) Koleske, D. D.; Barger, W. R.; Lee, G. U.; Colton, R. J. *Mater. Res. Soc. Symp.* **1997**, *464*, 377.
(13) McDermott, M. T.; Green, J. D.; Porter, M. D. *Langmuir* **1997**, *13*, 2504.
(14) (a) Kiely, J. D.; Houston, J. E.; Mulder, J. A.; Hsung, R. P.; Zhu, X.-Y. *Tribol. Lett.* **1999**, *7*, 103. (b) Bar, G. *Langmuir* **1997**, *13*, 373.
(15) (a) Clear, S. C.; Nealy, P. F. *J. Chem. Phys.* **2001**, *14*, 2802. (b) Wong, S.; Takano, H.; Porter, M. D. *Anal. Chem.* **1998**, *70*, 5209. (c) Liu, Y.; Evans, E. F. *Langmuir* **1996**, *12*, 1235.
(16) Lio, A.; Charych, D. H.; Salmeron, M. *J. Phys. Chem. B.* **1997**, *101*, 3800.
(17) Chaudhury, M. K.; Owen, M. J. *J. Phys. Chem.* **1993**, *97*, 5722.

10.1021/la049448u CCC: $27.50
Published on Web 08/19/2004

experiment, the adhesion behavior of monolayers might be inevitably affected by factors other than phase state changes, such as differing molecular structures (linear/branched, aliphatic/aromatic) and varying chain lengths.

With regards to the monolayer chain length, inconsistent results are often observed. For a probe (e.g., AFM tip) modified with a suitable monolayer, it was reported that adhesion/friction forces increase with increasing chain length due to more effective interdigitation between the surface monolayer and the modified probe.[9,10] However, in the case where an inorganic probe (e.g., Si_3N_4 tip) was used,[11−15] higher adhesion/friction forces were observed with decreasing chain length since short chains invariably form disordered monolayers with loosely packed structures. Here, the decreasing chain length facilitates molecular contact between the inorganic probe and the monolayer due to the increased ease of surface penetration by the probe into the loosely packed monolayer, resulting in a subsequent increase in the contact area. However, even for the same chain lengths and surface functionality, the different adhesion/friction behavior were observed depending on the types of SAMs.[16] For monolayers of *n*-alkyltrichlorosilanes and alkylthiols, the degree of molecular ordering is different even for monolayers of the same chain length, which is thought to be responsible for the different adhesion/friction behavior.

In summary, the physical factors involved in the nanoadhesion/friction behavior of monolayers are dependent on one another. Longer chains usually give rise to ordered and highly packed monolayers, whereas for shorter chains, packing density becomes low; thus, disordered monolayers are formed. Morever, significant reduction in molecular packing density causes the surface heterogeneity.[17] The surface heterogeneity resulting from the uncovered (bare) substrate can also have a significant effect on the adhesion/friction behavior. However, while the nanoadhesion behavior of monolayers has been intensively studied, the effect of their phase state on adhesion strength while maintaining the chain length and surface heterogeneity the same, has yet to be investigated at the molecular level. Consequently, the design of a suitable experiment to elucidate the effect of phase state on nanoadhesion behavior is desirable.

SAMs of *n*-alkyltrichlorosilanes are highly suited for elucidating the effect of phase state on nanoadhesion behavior since they have transition temperatures, at which their chain conformation can be changed.[18−20] Monolayers with various structures (ordered/disordered) induced by chain conformation changes can be formed simply by adjusting the deposition temperature. Here, we report the effect of *n*-alkyltrichlorosilane monolayer phase changes on their nanoadhesion properties by controlling their chain conformation while excluding the influences of chain length and surface heterogeneity. Here, we focus on the mechanical deformation of molecularly thin films, which have the same surface energy but different chain structures, in an attempt to relate this to nanoscale adhesion.

Experimental Section

Materials. Octadecyltrichlorosilane [$CH_3(CH_2)_{17}SiCl_3$, C-18], octyltrichlorosilane [$CH_3(CH_2)_7SiCl_3$, C-8], and anhydrous toluene (Aldrich) were used as received. All alkylsilane materials and anhydrous toluene were stored in a desiccator prior to use. P-type Si(100) wafers (Shinetsu) were cleaned in piranha solution (70% vol H_2SO_4 + 30% vol H_2O_2) for 30 min at 100 °C washed with copious amounts of distilled water, and stored in a vacuum prior to use.

Monolayer Deposition. Vacuum-dried reaction flasks were charged with anhydrous toluene and cleaned Si wafers under argon. The flasks were then placed in a temperature-controlled bath and allowed to stand for 30 min to ensure thermal equilibrium. Alkyltrichlorosilanes were then added to the flask (10 mM) and left to self-assemble on the wafers for 2 h under argon. The silicon wafers were removed from the alkyltrichlorosilane solution, rinsed with toluene and ethanol for several times, and then baked in oven at 120 °C for 20 min. After baking, the substrates were cleaned by ultrasonication in toluene and rinsed thoroughly with toluene and ethanol followed by vacuum drying prior to use.

Surface Characterization. Monolayer thickness was determined using an ellipsometer (M-2000V, J. A.Woollam Co., Inc.), while the chain conformation was investigated by analyzing the absorption spectra obtained from a Fourier transform infrared spectrometer (FT-IR, Bruker IFS 66v), using p-polarized light with an incident angle of 80°. Surface wettability was determined by measuring the contact angle formed between a probe liquid (distilled water or hexadecane) and the monolayer surface using a contact angle meter (Krüss BSA 10). The monolayer surface topography was examined by atomic force microscopy (AFM) (Autoprobe CP, Park Scientific Instruments). AFM images were obtained in contact mode, using silicon nitride cantilevers with a force constant of 0.1 N/m, and a scan rate of 1.0 Hz.

Adhesion Force Measurements. Adhesion forces were measured between the AFM tip (Si_3N_4) and SAMs by recording the cantilever deflection in the force−displacement (attraction−retraction) curves. AFM experiments were performed at a relative humidity controlled within the range 25−35% under a nitrogen atmosphere. The magnitude of the pull-off jump in the retraction portion of the force−displacement curve corresponds to the adhesion force. The tip scanning speed was maintained at 1 μm/s, with an applied force of 1 nN. To minimize the variability of the tip shape, the same tip was used throughout the investigation. Reliable pull-off force measurements were obtained by averaging 10 data points per sample by recording the force−displacement curves at different locations on the surface.

Adhesion Energy Measurements. The adhesion energy was measured using a homemade JKR apparatus on the basis of contact mechanics.[22−25] Briefly, the instrument comprises three main components—an electrobalance (to record the contact force), an optical microscope (to monitor the contact radius), and a manipulator (to control the probe). The JKR apparatus is placed on a vibration-isolation table and housed within a humidity-controlled chamber. All JKR experiments were performed under a nitrogen atmosphere, with a relative humidity between 25 and 35%. A cross-linked poly(dimethylsiloxane) (PDMS) (Sylgard 184, Dow Corning) hemispherical lens (of diameter 1 mm) was fabricated according to literature methods.[25,26] From the initial contact, the probe lens was lowered 6 μm with a loading rate of 20 nm/s, while the unloading rate was varied from 20 to 5 μm/s.

Results and Discussion

Structure of SAMs. Characteristic IR peaks resulting from the methylene (−CH_2) stretching vibrations of well-ordered monolayers (ca. 2920 cm^{-1}) were observed for the C-18 monolayers deposited below 30 °C. These characteristic peaks exhibit an upward shift as the deposition temperature was increased (Figure 1A), indicating that the ordered, mainly trans-conformation chain structures

(18) (a) Iimura, K.; Nakajima, Y.; Kato, T. *Thin Solid Films* **2003**, *379*, 230. (b) Rye, R. R. *Langmuir* **1997**, *13*, 2588.
(19) Brzoska, J. B.; Azouz, I. B.; Rondelez, F. *Langmuir*, **1994**, *10*, 4367.
(20) Parikh, A. N.; Allara, D. L.; Azouz, I. B.; Rondelez, F. *J. Phys. Chem.* **1994**, *98*, 7577.
(21) Girifalco, L. A.; Good, R. J. *J. Phys. Chem.* **1957**, *61*, 904.
(22) Chaudhury, M. K.; Whitesides, G. M. *Science* **1992**, *255*, 1239.
(23) Ahn, D.; Shull, K. R. *Macromolecules* **1996**, *29*, 4381.
(24) Deruelle, M.; Leger, L.; Tirrell, M. *Macromolecules* **1995**, *28*, 7419.
(25) Chaudhury, M. K.; Whitesides, G. M. *Langmuir* **1991**, *7*, 1013.
(26) Efimenko, K.; Wallace, W. E.; Genzer, J. *J. Colloid Interface Sci.* **2002**, *254*, 306.

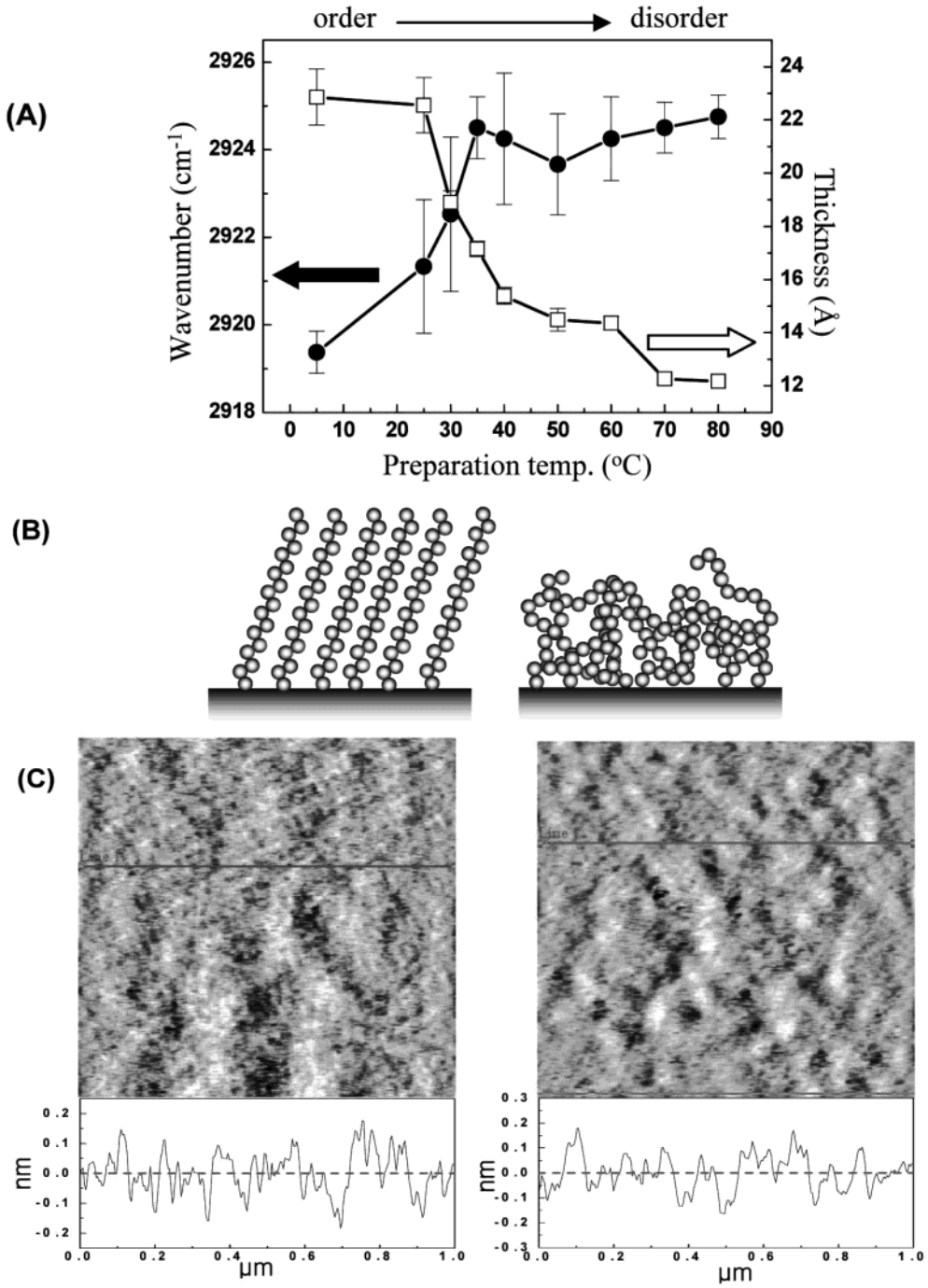

Figure 1. Molecular structures of C-18 monolayers deposited at various temperatures: (A) Changes in the CH_2 asymmetric vibration (solid) and thickness (open) of monolayers with respect to the deposition temperature. (B) Schematics representing monolayers in both ordered (left) and disordered (right) phases. (C) AFM images of ordered (left, deposited at 5 °C) and disordered (right, deposited at 50 °C) monolayers (rms roughness is ~1 Å irrespective of deposition temperature).

transform into disordered structures with increasing gauche defects.[18] The monolayer thickness determined by ellipsometry (Figure 1A) shows a steep decrease around 30 °C. This result coincides with the IR observations, implying that a reduction in the monolayer thickness corresponds to an increase in structural disorder. From these results, it is concluded that C-18 monolayers have a transition temperature (T_c) around 30 °C, which is in good agreement with previous reports.[18−20] The structure of monolayers having different chain conformations is schematically represented in Figure 1B.

The surface morphologies of the C-18 monolayers were found to be both homogeneous and smooth (roughness ~1 Å), irrespective of the monolayer chain conformation, as confirmed by AFM (Figure 1C). The corresponding surface wettabilities (obtained from contact angle measurements) were essentially the same for all monolayer surfaces (Table 1). From these results, we can conclude that the silicon substrates showed complete coverage by C-18 monolayers for all cases and that the molecular density of the monolayer was not sufficient to alter the surface properties.

Adhesion Force. The adhesion force/energy, molecular deformation, and relaxation behavior of the C-18 monolayers were investigated by AFM and JKR analyses. Parts A and B of Figure 2 show the results obtained from AFM force−displacement curves (Si_3N_4 tip) for C-18 monolayers deposited at various temperatures. Interestingly, striking

Table 1. Surface Wettabilities of C-18 Monolayers Deposited at Various Temperatures, Using Pure Water and Hexadecane as Probe Liquids.[a]

preparation temperature (°C)	5	25	30	40	50	60
contact angle (water)	106	106	104	102	102	102
contact angle (hexadecane)	40	40	40	38	36	36
surface energy (mJ/m^2)	21.5	21.5	21.5	22.1	22.6	22.6

[a] Surface energies of monolayers were calculated from the hexadecane contact angles using the equation of Good-Girifalco and Fowkes[21], $\gamma_{sv} = \gamma_{lv}(1 + \cos\theta)^2/4$

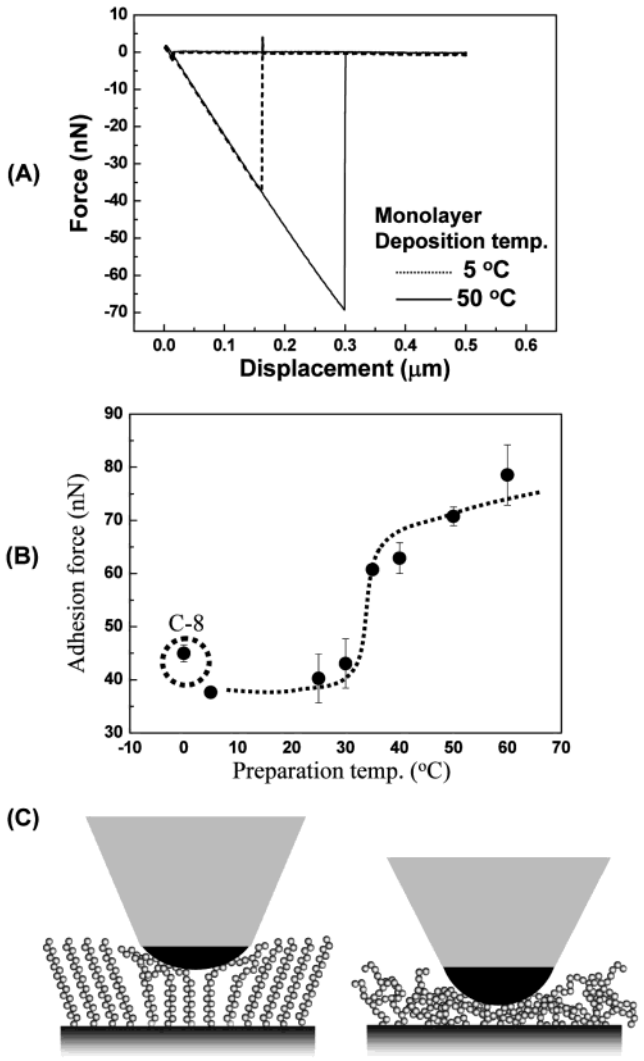

Figure 2. Adhesion forces of SAMs. (A) Representative force−displacement curves obtained from AFM for SAM with different deposition temperature. (B) Adhesion (pull-off) forces between the AFM tip and C-18 monolayers of various chain conformations (adhesion force for ordered C-8 monolayer is included, circular dots). (C) Schematic illustrating the moment of contact between an AFM tip and monolayers of ordered (left) and disordered (right) phases, where the increased contact area for disordered monolayers is due to the more-deformable structure.

differences in the adhesion forces were observed around the transition temperature of the monolayer (~30 °C), where conformational changes were observed.

Interdigitation is not possible in this case, since only inorganic AFM tips are used. Furthermore, mechanical interlocking between the Si_3N_4 tip and the C-18 monolayer is negligible since the curvature of the tip is extremely small (~50 nm). Additionally, long-range van der Waals interactions between the Si_3N_4 tip and the silicon wafer are also expected to contribute to the attractive forces. The distance between the tip and wafer in the case of ordered C-18 monolayers is ca. 2.5 nm, whereas it is less than 1.5 nm when the same monolayers are disordered. The tip−surface distance for disordered monolayers may be even less due to the possible penetration of the tip into the monolayers. Thus, there is a further possibility that the Si_3N_4 tip, which has a higher surface energy than most organic materials, experiences stronger attractive forces toward the silicon substrate as the monolayer film thickness decreases. To ascertain the effect of the long-range van der Waals interaction originated from the distance between the tip and the silicon substrate, the short chain alkyltrichlorosilane, such as octyltrichlorosilane (C-8), having an ordered state, was deposited on the wafer at −10 °C. The FT-IR (ca. 2850/2920 cm^{-1}) and ellipsometry results indicate that the C-8 monolayer has an ordered structure of thickness ~1.3 nm, a value very close to that of the disordered C-18 monolayer. However, the determined adhesion force for this ordered C-8 monolayer is comparable to that of the ordered C-18 monolayer with much larger layer thickness (Figure 2B). This result suggests that the disordered C-18 structure, induced by chain conformation changes, is the main factor involved in molecular contact and adhesion enhancement.

Consequently, the true contact area must be ascertained for all cases in order to verify the increases in adhesion force. This value cannot be measured directly by AFM but can only be inferred from the properties of the materials studied. This is one of the demerits of the AFM force−displacement mode. In this case, mechanical properties, such as the modulus or stiffness of the organic monolayer, become crucial factors in determining the contact area between the probe tip and monolayer.[27−29] Inorganic (Si_3N_4) tips have sufficient mechanical strength to penetrate an organic film, resulting in an increase in the contact area during tip approach. Therefore, as the monolayer structure becomes disordered and a weaker mechanical resistance is realized, the tip is able to penetrate deeper into the monolayer accompanied by a concomitant increase in contact area, as shown schematically in Figure 2C. Consequently, as the deposition temperature is raised (increasing disorder), the contact area increases, resulting in an enhanced adhesion force.

Adhesion Energy/Hysteresis. An increase in the adhesion force for disordered monolayers is typically accompanied by a corresponding increase in the contact area. Therefore, to ascertain the change in adhesion strength at the same contact area, the adhesion energy, or adhesion force relative to the true contact area, should be compared. However, the AFM force−displacement mode is disadvantaged in that true estimations of the tip geometry and contact area are difficult to establish, precluding quantitative analysis and determination of the adhesion energy from contact mechanics-based equations such as JKR and DMT.[30,31] The JKR apparatus on the other hand, predicts the adhesion energy (W) on the basis of contact mechanics from direct measurement of the curvature of the probe lens (R), the contact radius (a), and

(27) Chen, Y. L.; Helm, C. A.; Israelachvili, J. N. *Langmuir* **1993**, *7*, 2694.
(28) Leng, Y.; Jiang, S. *J. Chem. Phys.* **2003**, *113*, 8800.
(29) Quon, R. A.; Ulman, A.; Vanderlick, T. K. *Langmuir* **2000**, *16*, 3797.
(30) Johnson, K. L.; Kendall, K.; Roberts, A. D. *Proc. R. Soc. London A* **1971**, *324*, 301.
(31) Derjaguin, B. V.; Muller, V. M.; Toporov, Yu. *J. Colloid Interface Sci.* **1975**, *53*, 314.

the force (P). Equations based on the JKR theory have been applied throughout this study.

$$a^3 = \frac{R}{K}[P + 3\pi WR + (6\pi WR + (3\pi WR)^2)^{1/2}] \quad (1)$$

$$P_{\text{off}} = -\frac{3}{2}\pi WR \quad (2)$$

where

$$R = \frac{R_1R_2}{R_1 + R_2}, \quad K = \frac{4}{3}\left[\frac{(1-\nu_1^2)}{E_1} + \frac{(1-\nu_2^2)}{E_2}\right]^{-1},$$

ν = Poisson's ratio, P_{off} = pull-off force.

The JKR probe was constructed from unextracted PDMS in the form of a hemispherical lens (ca. 1 mm radius). The unextracted PDMS surface is composed of cross-linked networks and non-crosslinked free chains, having quite a smooth surface. Adhesion between this probe lens and C-18 monolayers of various chain conformations was investigated during both loading and unloading. In the loading process, the intrinsic work of adhesion (W) was obtained from eq 1 by successive measurements of the contact radius and force, while maintaining contact with the monolayer surface in the equilibrium state by moving the probe lens at a very slow rate (20 nm/s). From the initial contact, the lens was lowered by 6 μm. In the unloading process, the effective adhesion energy (G) was obtained from either eq 1 or eq 2, varying the detachment conditions (equilibrium/nonequilibrium) by adjusting the unloading speed from 20 to 5000 nm/s. It was found that fitting the procedure with a^3 and P using eq 1 and calculation with pull-off force using eq 2 generated very similar values of G for a low unloading rate (up to 200 nm/s). At much higher unloading rate, we could not obtain enough contact images to use eq 1. Thus, in the graph (Figure 4) showing the rate-dependent adhesion hysteresis, we used the adhesion energy calculated from pull-off force which can be easily determined from the force−displacement curve (maximum force before detachment).

Figure 3A shows the representative a^3-P curves for the ordered and disordered C-18 monolayer (unloading rate of 200 nm/s). As expected, similar intrinsic adhesion energies (W) were obtained during the loading process in all cases irrespective of the deposition temperature of monolayer, i.e., monolayer phase state. Furthermore, remarkable differences in the adhesion energies (G) were observed for the different monolayer phase states (Figure 3B). The adhesion hysteresis ΔW ($G - W$), a contribution from additional adhesion promotion besides the intrinsic interfacial interaction, was quantitatively analyzed in this study. The adhesion hysteresis arising between the probe lens and C-18 monolayers of various phase states is shown in Figure 3C. As in the AFM study, a substantial increase in the adhesion hysteresis is observed near the transition temperature. Here, however, the mechanically forced deformation of the monolayer by the soft elastic PDMS lens (ca. 1 MPa) is less likely to occur than if an inorganic AFM tip was employed. Moreover, the energy dissipation (Φ) at the probe−monolayer interface can be investigated by analysis of the adhesion hysteresis. The equation for the adhesion energy, [$G = W(1 + \Phi(v, T))$], indicates that the adhesion hysteresis ($G - W$) concerns only the irreversible changes at the interface during detachment of the probe from the surface since W is essentially constant irrespective of the monolayer phase, as shown in Figure 3B.

The mechanism for the increase in adhesion energy is completely different from the results obtained using AFM, as the effects of contact area on adhesion are minimal in this case. Due to the fact that attractive forces between PDMS and monolayers are nearly same regardless of phase states of monolayers and that the same PDMS lens was used throughout this study, changes in adhesion energy (hysteresis) are presumed to be mainly from the excess deformation of monolayers during the unloading process. The deformation of monolayer under the action of attractive force during unloading would become greater as the monolayer becomes more compliant. Consequently, as the preparation temperature is raised (increasing disorder), the monolayer changes to the mobile state with less stiffness, resulting in more excess deformation during unloading and, thus, an increased adhesion hysteresis.

The interdigitation effect, which usually has significant contribution to the adhesion energy, as mentioned before, can be also taken into consideration. Disordered monolayers are susceptible to interdigitation with PDMS chains, while ordered monolayers are not. Then, this interdigitation would cause further deformation of disordered monolayers during unloading besides interfacial force-induced deformation. In this case, the small-scale deformation of the PDMS lens would be also involved.

Thus, the difference in adhesion hysteresis for monolayers having different phase states might be a result of interdigitation and excessive monolayer deformation during unloading, two parameters related to the chain mobility of the monolayers. The more deformable states of the disordered monolayers, those which are vulnerable to the external forces applied by JKR probe lens, are highly susceptible to interdigitation upon loading and are capable of deformation following unloading. Thus, it can be said that increases in the adhesion hysteresis are promoted by the monolayer's ability to deform in response to changes in the chain conformation.

Experiments using shorter chain lengths (C-8) with ordered structures have also been performed (Figure 3B, C). The adhesion hysteresis value for the C-8 ordered monolayer is much lower than those of the disordered C-18 monolayers but similar to those of the ordered C-18 monolayers, which is in good agreement with the above explanation in terms of reduced deformation ability.

Rate Dependence of Adhesion Hysteresis. The deformation ability of monolayers is essentially related to the chain mobility. As the monolayer chains approach a more mobile state with increasing disorder, they are more likely to deform readily during the unloading process. The dependence of the adhesion hysteresis on the unloading rate was determined in order to investigate the effect of chain mobility (Figure 4), where the loading conditions were fixed (20 nm/s; 6 μm) to maintain the same conditions during contact. The maximum adhesion hysteresis, a parameter closely related to the chain-relaxation mobility, was observed in all cases.[9,33,34] This condition is characterized by the Deborah number (De), a number which corresponds to the ratio of the characteristic relaxation time with respect to the measurement time, such that when De has a value of ~1, the energy dissipation (hysteresis) is generally at a maximum. Adhesion hysteresis can be represented by dynamic (nonequilibrium) phase diagrams. For example, plots of energy dissipation (hysteresis) versus the loading−unloading rate (peeling

(32) Silberzan, P.; Perutz, S.; Kramer, E. J. *Langmuir* **1994**, *10*, 2466.
(33) Luengo, G.; Pan, J.; Heuberger, M.; Israelachvili, J. N. *Langmuir* **1998**, *14*, 3873.
(34) Israelachvili, J. N.; Berman, A. *Isr. J. Chem.* **1995**, *35*, 85.

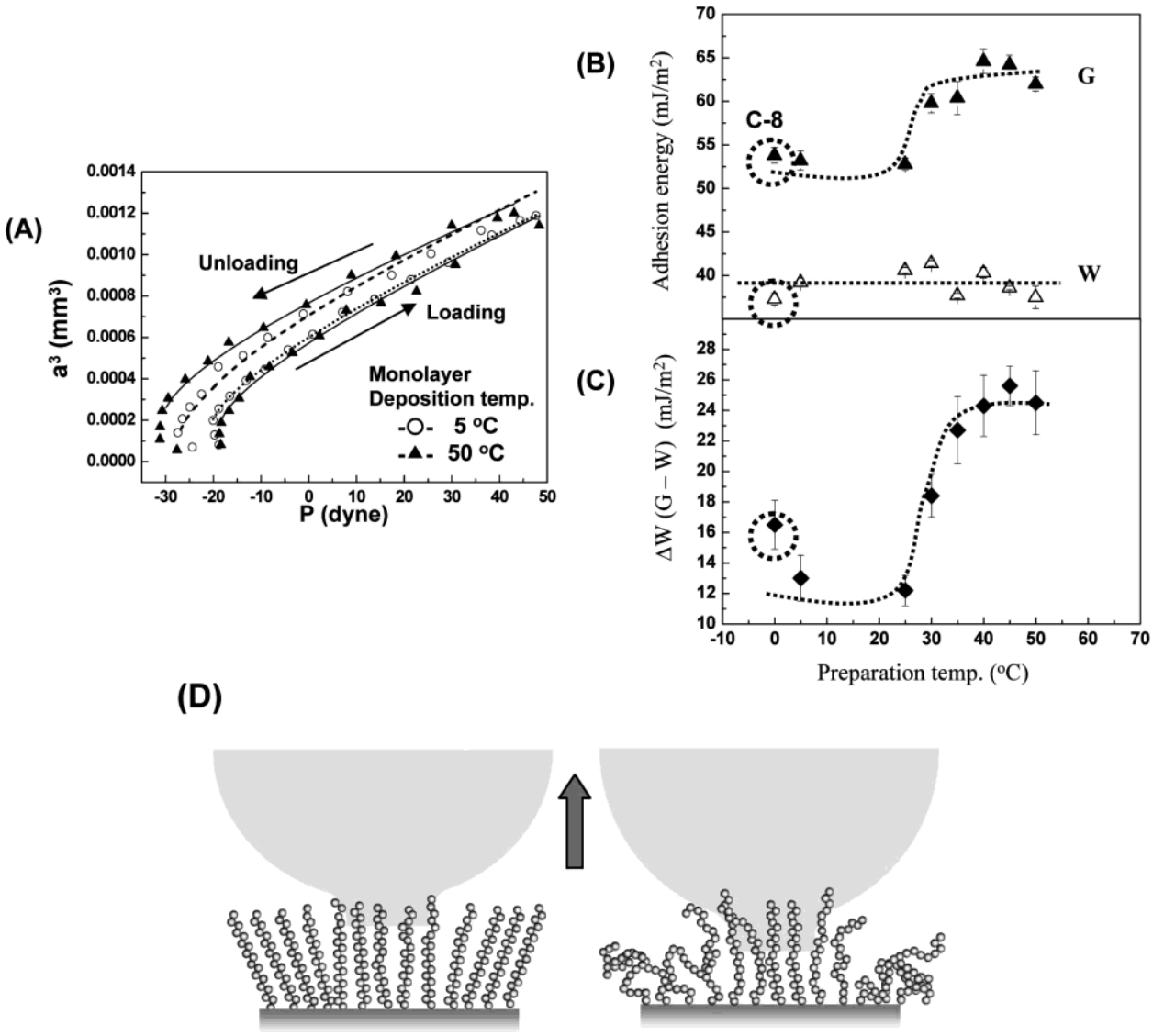

Figure 3. Adhesion energy/hysteresis of SAMs. (A) Representative a^3-P plot of loading/unloading cycles for C-18 monolayers obtained from JKR experiments. (B) Intrinsic work of adhesion (W, loading, 20 nm/s) and adhesion energy (G, unloading, 200 nm/s) between a PDMS lens and C-18 monolayers of various chain conformation. (C) Adhesion hystersis ($G - W$) obtained from Figure 2B. (W, G, and adhesion hysteresis of ordered C-8 monolayers are included, dot circle). (D) Schematic depicting the unloading process for ordered (left) and disordered (right) monolayers—increase in the excess deformation during the unloading process caused by the interdigitation of disordered monolayers with the PDMS lens.

rate) at constant temperature often peak at some critical rate or velocity when $De \approx 1$.

In this study, we found that when the unloading rates were slower than the chain relaxation rates the deformed monolayer chains had sufficient time to return to their previous undeformed state with minimal adhesion hysteresis. When the unloading rate exceeds the chain-relaxation rate, then the deformed chains are unable to return to their original state within the experimental time frame, resulting in an increased adhesion hysteresis. At the point where the unloading rate becomes too great, only the probe lens deforms and detaches from the surface prior to rearrangement of the chains in the monolayer, causing a decrease in the adhesion hysteresis. In Figure 4, the ordered C-18 monolayers exhibit only a marginal amount of adhesion hysteresis with respect to changes in the unloading rate (a). As the monolayer phase state becomes disordered with increasing deposition temperature, the amount of hysteresis increases, and the maximum peak becomes more prominent. Furthermore, the observed shift in maximum hysteresis toward higher

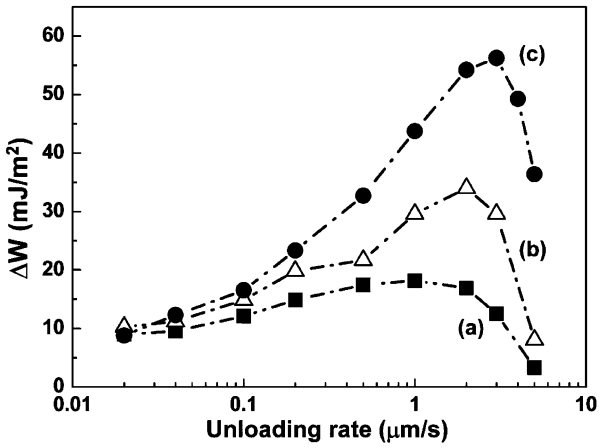

Figure 4. Rate dependence on adhesion hysteresis of C-18 monolayers deposited at (a) 5 °C, (b) 30 °C, and (c) 50 °C, respectively. As the monolayer phase approaches a disordered state, the adhesion hysteresis increases, with maximum hysteresis occurring at higher unloading rates.

rate evidences that the disordered monolayer has greater mobility and deformation ability during unloading.

As well as contributions from the monolayer chains, it should also be noted that the rate-dependent behavior of adhesion hysteresis might also derive from the bulk or interfacial chains of the probe material (PDMS). The degree of adhesion hysteresis is also potentially dependent on other physical states of the JKR probe lens, such as the amount of free chains at the surface[35] and their respective molecular weights,[36] as well as the size of the probe lens. However, the general trend in adhesion hysteresis with respect to the monolayer phase state remains the same. Considering that the same lens was used throughout the experiment and that maximum hysteresis shifts toward higher rate for the disordered monolayer, the increase in adhesion hysteresis for disordered monolayers is thought to result from molecular deformation of the monolayer chains during the unloading process.

On the basis of the results shown in Figure 4, it is speculated that the amount of deformation energy contributed to the adhesion strength by way of induced chain conformation changes in the monolayer can be as high as 40 mJ/m^2 (at the point of maximum hysteresis).

Comparison of AFM and JKR Experiments. AFM and JKR techniques have been employed to investigate the adhesion behavior of SAMs at the molecular level. The main difference between the two techniques is essentially the material and geometry of probe; AFM relies on sharp and rigid tips such as Si_3N_4, while JKR uses an organic flexible lens constructed from polymeric materials. In this study, AFM sensed subtle changes in mechanically deformed contact areas using a less-deformable inorganic tip. Hence, the number of monolayer chains in contact with the tip differs depending on the phase state of the monolayer, as previously discussed (see also Figure 2C). In the JKR method, the use of flexible lenses to measure the adhesion strength (in units of energy per area) overcame the demerits of the AFM experiment. However, it should be noted that viscoelastic deformation of the lens is always involved, making it difficult to obtain an absolute value for the adhesion hysteresis of the monolayer itself. Similar adhesion hysteresis values (ca. 10 mJ/m^2) are observed for the C-18 monolayer irrespective of the phase state during the unloading condition at very slow rates (Figure 4). Small, comparable adhesion hysteresis values obtained at the slowest rate (20 nm/s) are likely to result from bulk deformation of the JKR probe lens, assuming that the monolayer chains (both ordered and disordered) have enough time to undergo relaxation. In this experiment, the viscoelastic deformation of the PDMS lens was not sufficient to mask the contribution of the monolayer deformation to the adhesion hysteresis.

It is worth mentioning that the sensitivities of the AFM and JKR instruments are essentially quite different in value. The AFM senses force in the scale of nN according to tip deflections when contact with the substrate of which the motion is controlled in the sub-nanometer range, while the JKR apparatus measures force (electrobalance) and contact radius (optical microscope) with sensitivities of the order μN (10^{-5} g) and μm, respectively. The AFM has a significant advantage over the JKR apparatus in the measurement of adhesion forces at the molecular scale since slight changes in the physical or chemical state can be detected with a high degree of sensitivity. The JKR apparatus on the other hand measures adhesion strength in terms of energy, where both equilibrium (intrinsic work of adhesion) and nonequilibrium (effective adhesion energy) properties can be obtained simultaneously. Moreover, various time-dependent interfacial phenomena can be predicted from these results.

The contact area for the JKR experiment is typically much larger (more than tens of microns) than that employed in AFM measurements and yields averaged information regarding the interface between the probe and surface. Equation 2 has meaningful implications in that the scale is irrelevant in evaluating the adhesion energy. Measurement of the adhesion force on a larger scale can be overcome by using larger-sized materials. Consequently, the measurement scale in JKR experiments was well suited for this particular study since the monolayer phase change contribution to the adhesion hysteresis was not masked by the deformation of the probe lens and could be observed successfully without loss of accuracy in the adhesion energy measurement, owing to sufficient resolution of the optical microscope and electrobalance components in the JKR apparatus.

Conclusions

Self-assembled monolayers (SAMs) of equal chain length and different phase state induced by chain conformation changes without any surface heterogeneity have been used to demonstrate the effect of chain conformation change on nanoadhesion behavior using a combination of AFM and JKR methods. The adhesion force/energy was found to increase as the monolayer phase changed from an ordered to a disordered state. This can be explained in terms of the molecular deformation ability of monolayers: (1) an increase in molecular contact between the AFM tip and a disordered monolayer due to the more deformable state of the latter and (2) monolayer deformation during unloading by the JKR probe lens. Adhesion hysteresis was found to be more sensitive to the unloading rate for disordered monolayers. The occurrence of maximum hysteresis at faster rates proves that monolayer chain mobility increases with disordered structure, resulting in increased mechanical deformation.

Acknowledgment. The authors thank the Ministry of Science and Technology of Korea (National Research Laboratory Project) and the Ministry of Education of Korea (BK21 Program) for their financial support.

LA049448U

(35) Amouroux, N.; Leger, L. *Langmuir* **2003**, *19*, 1396.
(36) Choi, G. Y.; Zurawsky, W.; Ulman, A. *Langmuir* **1999**, *15*, 8447.